Research Article

Effects of geometrical and processing parameters on mechanical properties of auxetic polyurethane foams

Navid H. Z. Abedini[1] · Amir Nourani[1] · Mahdi Mohseni[1] · Nesa Hosseini[1] · Sepideh Norouzi[1] · Parsa Riazi Bakhshayesh[1]

Received: 14 October 2021 / Accepted: 22 April 2022
Published online: 10 May 2022

Abstract
This study aimed to investigate the influence of processing parameters on the mechanical properties of auxetic polyurethane foams including Poisson's ratio and Young's modulus. 12 different processing scenarios were considered using the method of Plackett–Burman in the design of experiments with three replicates for each one. Eventually, 36 foams were prepared with different densities and initial thicknesses, heating temperatures and times, applied compression ratios, and the rest times between two heating steps. The microstructures of the conventional and auxetic samples were observed by scanning electron microscopy (SEM). All samples were subjected to tensile loading in one direction with two different strain values. The strains of the foams in two other directions were recorded using a digital image correlation method. Also, the required force to create each strain value was recorded. The results showed that depending on the changing parameters, Poisson's ratio of about 42% and 58% of the samples reduced at the strains of 10% and 20%, respectively. Heating temperature and time, the initial thickness of the foam, and the applied compression ratio were proved to have significant effects on the variations of both Poisson's ratio and Young's modulus of the foams. It was concluded that the Poisson's ratio of foams was reduced at higher heating temperature, time, and applied compression ratio and also a lower foam initial thickness. On the other hand, these changes increased Young's modulus of the polyurethane foams. The strain energy of the auxetic samples showed higher amounts of energy compared to the other foams.

Article highlights

- The thermo-mechanical procedure was used to manufacture auxetic foams.
- Effect of processing parameters on the foam mechanical properties was investigated.
- Foams Poisson's ratio and Young's modulus were measured in two strain values.

Keywords Polyurethane foam · Poisson's ratio · Young's modulus · Auxetic materials · Processing parameters · Thermo-mechanical procedure

✉ Amir Nourani, nourani@sharif.edu; Navid H. Z. Abedini, n.hajizeinolabedini75@student.sharif.ir; Mahdi Mohseni, mahdi.mohseni@mech.sharif.edu; Nesa Hosseini, nesa.hosseini111@sharif.ir; Sepideh Norouzi, Sepideh.noroozi2015@student.sharif.ir; Parsa Riazi Bakhshayesh, parsa.riazi@mech.sharif.edu | [1]Department of Mechanical Engineering, Sharif University of Technology, Tehran, Iran.

Abbreviations

CR	Compression ratio
D_c	Percentage of change in foam density
E	Young's modulus
PU	Polyurethane
T_0	Foam initial thickness
T_i	Heating time
T_f	Foam final thickness
ε_y	Strain of y direction
v	Poisson's ratio
v_{xz}	Poisson's ratio in z direction
D_0	Foam initial density
D_f	Foam final density
F	Applied tensile load
RT	Rest time
T_e	Heating temperature
T_c	Percentage of change in foam thickness
ε_x	Strain in x direction
ε_z	Strain in z direction
v_{xy}	Poisson's ratio in y direction

1 Introduction

Poisson's ratio, *v*,is one of the most important characteristics of materials. It is defined as the negative transverse strain divided by the axial strain. Most of the regular materials have positive *v* values, while *v* values of auxetic materials are negative. A negative *v* would cause materials to yield special properties such as superior energy absorption, causing broad applications of these materials in sports apparel [1] and fenders [2]. Also, they have high values of strain energy release rate which results in a higher amount of fracture toughness [3]. This property is of great importance in fabricating shock absorbers and fasteners [4]. Also, several numerical studies have shown that auxetic materials can be used for applications that require high energy absorption [5, 6].

Auxetic materials first were reported in 1987 with some experiments on isotropic open-cell foams [7]. Also, the *v* for different materials was observed to vary in the range of 0–0.5. Love [8] reported a *v* of − 0.14 for single-crystal pyrite. Lakes [7] triaxially compressed an open-cell polyhedron foam that resulted in inward bulking of the cell ribs and formation of the "re-entrant" structure in the foam. The compressed foam was placed in a mold at a temperature of 163–171 °C and then it was cooled down at room temperature. This procedure made a permanent transformation of open-cell foams to re-entrant structures [7].

Later, Evans and Alderson [9] claimed that this property could be found in both natural and artificial materials or could be seen in auxetic geometrical structures. Natural auxetic substances such as arsenic, bismuth, and cadmium were found auxetic by applying stress in their longitudinal direction and evaluating the lateral strain [10, 11]. Negative *v* was also observed in cube elemental metals (BCC and FCC crystalline lattices) when they have subjected to tensile loading at [110] direction [12]. In 1992, Haeri et al. [13] reported that the alpha-cristobalite molecular structure is a mechanism responsible for auxetic behavior in materials. They obtained this mechanism by the rotation of SiO_4 tetrahedral units [13]. Moreover, some of the biomaterials such as the load-bearing cancellous bone are known as natural auxetic materials [14]. Keyed brick [15] and polyurethane (*PU*) foams after specified thermo-mechanical procedures are some examples of artificial auxetic materials [16–18] and 2D re-entrant metamaterials are an example of auxetic geometrical structures [19].

Auxetic foams are generally manufactured under a thermo-mechanical process using conventional and common open-cell *PU* foams [20]. To investigate the effects of processing parameters on the *v* value of materials, Bianchi et al. produced an auxetic foam using a thermo-mechanical method [21]. They tested cylindrical *PU* foam samples with different initial diameters at varying heating and cooling conditions with different Compression ratios (*CR)* defined using the following equation:

$$CR = \frac{|Initial\ valume\ of\ foam - Final\ valume\ of\ foam|}{Initial\ valume\ of\ foam} \quad (1)$$

They reported that *v* values ranged from − 0.09 to − 0.63. It was concluded that *CR* had the most significant effect among the processing variables on the *v* value. The maximal temperature level and cooling method did not significantly affect the amount of *v* [21].

Li and Zeng [22] developed a low-cost, environmentally friendly, and ultra-fast method to build auxetic foams; a *PU* foam was compressed in a pressurized tank by spraying the CO_2 gas in the selected pressure and temperature. So, the distance between the foam particles is reduced. After releasing the pressure, this deformation became permanent to form an auxetic structure with a negative *v* of about − 0.5. Also, it was concluded that the tensile strain value in the range of 0–0.5 had no significant effect on the *v* value [22].

PU foams also, in turn, show different mechanical properties under different conditions. Constantinescu and Apostol [23] analyzed the effect of temperature and strain rate variation on stress response of polyurethane rigid foams under compressive tests and found that at a strain of 60%, these two parameters did not significantly affect the stress response of these foams with a density of less than 93 kg/m^3. However, low temperatures and high speeds of testing were found to cause an increase in the absorbed strain energy of polyurethane rigid foams with a density of 200 kg/m^3. Deschanel et al. reported tensile failure experiments on polyurethane foams. They showed

that the acoustic energy changes as a power of the foam density and/or temperature [24]. Linul et al. investigated the influence of density and loading direction (in-plane or out of plane) on main mechanical properties of polyurethane rigid foams such as Young's modulus and yield strength. They found that these mechanical properties increase significantly with increasing of density [25].

One of the most common thermo-mechanical processes of manufacturing auxetic *PU* foams is the thickness compression method [26]. This process consists of three main steps including mechanical compression, heating the compressed foam to its softening temperature, and cooling down the foam to maintain its new structure [27]. In this process, the microscopic structure of the foam was shown to be transformed from a semi-regular arrangement with straight and interconnected cell ribs to a denser, more compact, and tortuous cell structure. In this structure, the ribs could rotate around the corners [28–30].

As shown in the studies mentioned above, several parameters are involved in manufacturing auxetic foams that could affect the final mechanical properties of the foams. These parameters include applied *CR*, the heating temperature (T_e) and heating time (T_i) of the process for the compressed foams, the rest time (*RT*) between two heating steps, and also the foam initial thickness (T_0) and foam initial density (D_0). Previous studies reported inconsistent results on the effects of parameters such as T_e on the *v* and Young's modulus (*E*) for the processed *PU* foams [21, 31–33]. On the other hand, these studies did not investigate the interactional effects of these parameters on each other that could affect the final mechanical properties of processed *PU* foams. Also, the effects of D_0, T_0, and the *RT* on the final properties of the foams have not been investigated. Therefore, this work aimed to investigate the effects of all of the mentioned parameters on the mechanical properties of *PU* foams (i.e. *v* values in two directions and *E* values of the processed *PU* foams).

2 Materials and methods

2.1 Obtaining the softening temperature

Open-cell *PU* foams (Roya mattress corporation, Tehran, Iran) with D_0 of 20 or 40 kg/m^3 were used as the conventional foams. These foams were proved to experience four main steps in the heating process; glassy temperature, softening temperature, flow temperature, and breakdown temperature. The softening would be reached in temperature between the glassy and flow temperatures. In the softening state, the foam showed the elastic–plastic behavior and after reaching the flow temperature, the foam entered the plastic state [27].

Three heat tests were performed to obtain the softening temperature of the foam using a smart digital oven (Parsazma Co., Tehran, Iran). The specimens of *PU* foam of 60 × 150 mm with a thickness of 5 mm were placed in the oven. In the first case, the temperature was increased from 150 °C with an average rate of 5 °C/min and the foam condition was monitored every minute. At 230 °C, some deformation (i.e. shrinking) of the foam was observed. The second sample was placed at 180 °C and heated up to 220 °C with an average rate of 2 °C/min. A lower thermal rate (1 °C/min) also yielded the same outcome as the rate of 2 °C/min did. Finally, it was obtained that the softening temperature was about 220 °C and the thermal rate had no effect on it.

2.2 Design of experiments

Two parameters describing the initial foam characteristics including D_0 and T_0 were examined. Also, four parameters related to the manufacturing process including T_e, T_i, *CR* applied to the foams and the *RT* at room temperature between the two steps of oven placement were

Table 1 The list of experiments was designed using the Plackett–Burman method

Test No	D_0 (kg/m^3)	T_e (°C)	T_i (Min)	T_0 (mm)	*CR* (%)	*RT* (Min)
1	40	150	20	5	60	20
2	20	200	40	20	40	20
3	20	150	40	20	60	10
4	40	200	40	5	60	20
5	20	150	20	20	60	20
6	20	200	40	5	60	10
7	20	150	20	5	40	10
8	20	200	20	5	40	20
9	40	150	40	20	40	20
10	40	150	40	5	40	10
11	40	200	20	20	60	10
12	40	200	20	20	40	10

investigated. Table 1 lists the parameters with their values tested. 12 different experiments were designed using the Plackett–Burman method, and three replicates were considered for each test (Table 1).

2.3 Thermo-mechanical procedure

All the specimens were cut into rectangular shapes and prepared for the tests [34]. The schematic of the prepared samples is shown in Fig. 1a. A compression device of aluminum was built to compress the foams (Fig. 1b). As shown in Fig. 1a, the *x*, *y,* and *z* axes were defined in the directions of length, width, and thickness of the samples, respectively. Each test sample was first compressed through the z direction as shown in Fig. 1c. The distance between the two plates of the pressure device was measured by a caliper to gauge the amount of compression for all four sides of the specimen to apply a uniform pressure. Then, the whole set was placed in the preheated oven with the desire T_e. After reaching the T_i, the device and foam were removed from the oven, and also the pressure was released from the foam for the *RT* at room temperature. Previous studies showed that the cooling method did not affect the final mechanical properties of foams [21, 31]. Finally, the entire mechanism including the foam was placed again in the preheated oven at a temperature of 50 °C below that of the first heating step for the same time duration as done for the first heating step [26] (Fig. 2).

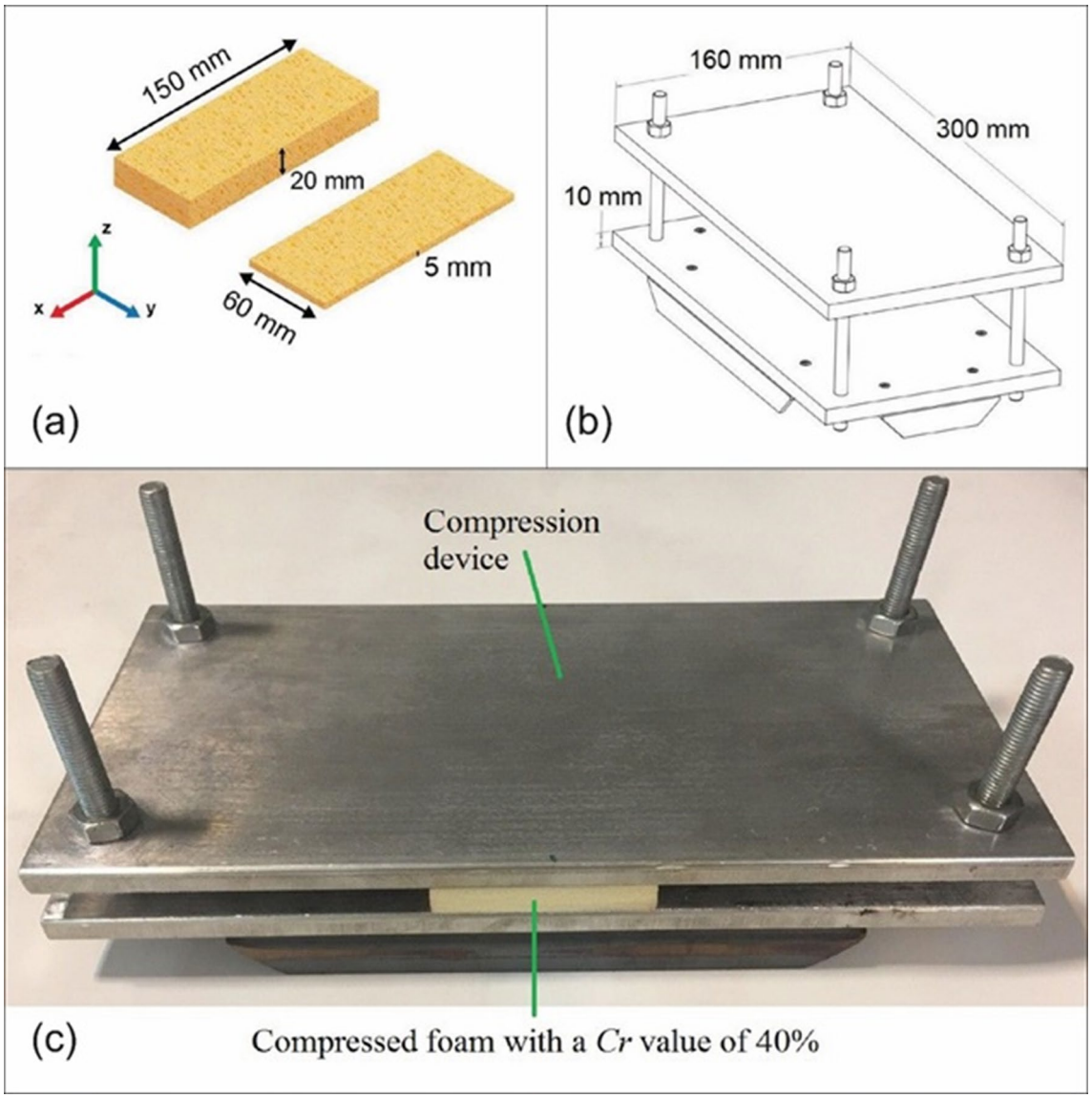

Fig. 1 **a** Schematic of samples with different initial thicknesses. **b** Schematic of the designed compression device. **c** The compression device with the compressed foam

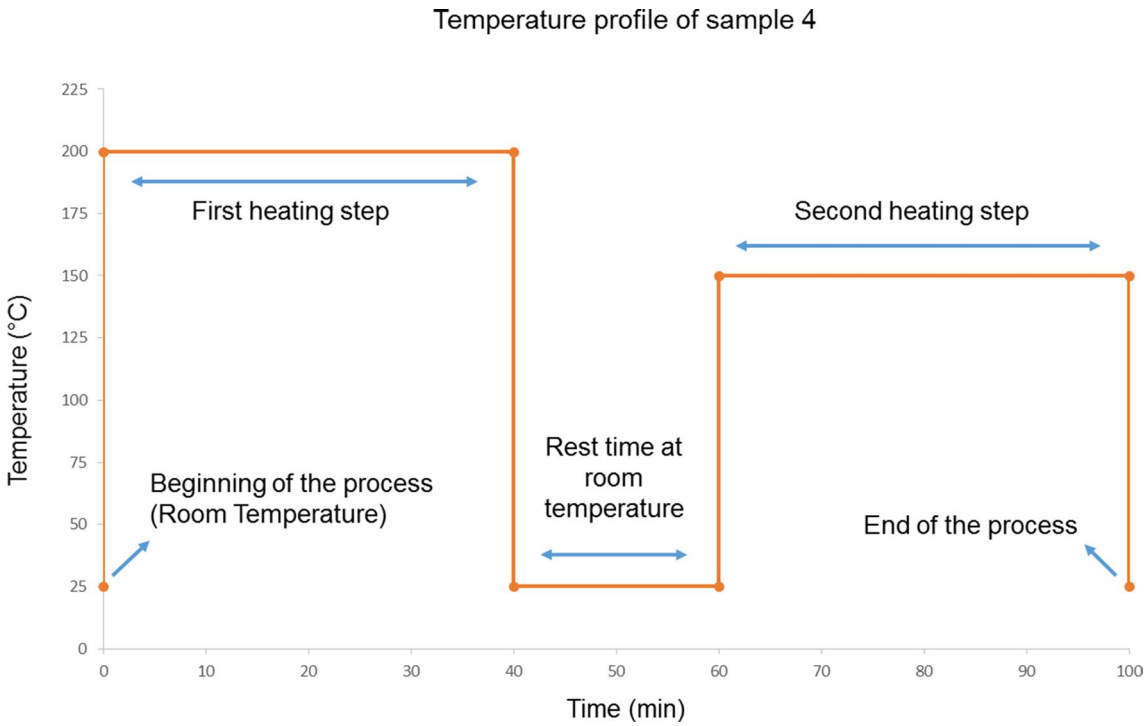

Fig. 2 Thermal profile of the process for test No. 4 from the beginning to the end of it

2.4 Mechanical testing and data acquisition

Two fixtures were made to attach the samples to the tensile test machine. All the specimens were lined at both ends equally (i.e. 10 mm) and located precisely in the fixtures (Fig. 3a). They were then subjected to tensile loading utilizing a Zwick-Roell Amsler HCT 25-400 tensile testing machine with a maximum load-cell capacity of 20 kN. Tests were performed with a cross-head speed of 5 mm/s to attain either final strain values of 10% or 20% in the x direction (ε_x).

The amount of strains in *y* direction (ε_y) and *z* direction (ε_z) were measured using the digital image correlation (DIC) method (GOM Correlate software, GOM Metrology Co., Schmitzstraße 2, 38,122 Braunschweig, Germany). In this method, a part of the specimen through its thickness and a part of the surface of the foam was painted with a black marker and a stochastic pattern was created to track foam strains in these two directions (Fig. 3b). The specimens were video recorded at 60 frames per second in both y and z directions during the tests (Fig. 3c). The camera had a 20-megapixel resolution with a focal length of 18–135 mm. The strain results of all three directions obtained from the DIC method were validated by measuring some of the dimensions of the loaded specimen randomly using a digital caliper.

2.5 Statistical analysis methods

The 95% confidence intervals of the results were calculated using Student's t distribution because each test was repeated three times. Also, the factorial analysis and ANOVA general linear model methods were used to analyze the differences between results and investigate whether the differences were significant. Finally, a *P* value lower than 0.05 was considered statistically significant.

3 Results

The outputs of the experiments were micrographs of the conventional and processed foams, the final thickness of foams, the amount of ε_y, ε_z, and also the amount of applied tensile load (*F*) applied on the processed samples to reach the desired ε_x values. Moreover, strain energy was calculated for all specimens.

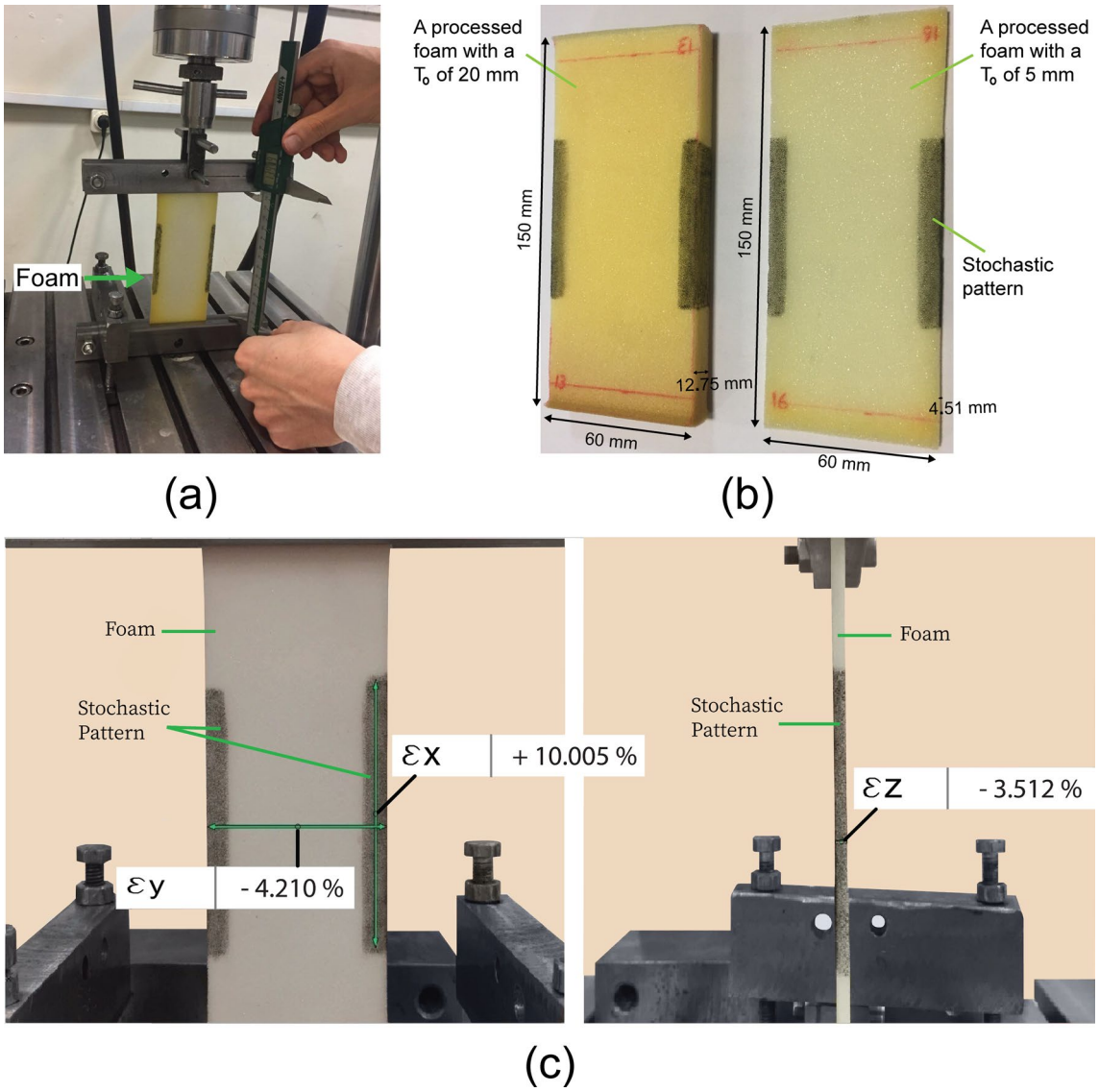

Fig. 3 **a** Placing the specimen in the tensile test machine. **b** Two processed foams with stochastic patterns and different thicknesses to track their dimensional changes during the tensile test. **c** Using the DIC method to obtain the ε_x, ε_y, and ε_z

3.1 SEM examination

Figures 4 and 5 show SEM micrographs of the conventional and processed foam of No. 6 (see Table 1), which had negative v (see Table 2), in two x–z and x–y planes. It can be seen in Fig. 4 that the quasi-regular convex-shape microstructure of the conventional foam has turned into a complex concave-shape with inwardly-buckled cell walls like re-entrant auxetic structure as Duncan et al. mentioned and, consequently, a negative v was observed [28]. Figure 5 shows no significant change other than a density increase.

3.2 Mechanical properties

The Poisson's ratios in the y direction (v_{xy}) and z direction (v_{xz}) were defined using the following equations:

$$v_{xy} = -\varepsilon_y/\varepsilon_x \tag{2-1}$$

$$v_{xz} = -\varepsilon_z/\varepsilon_x \tag{2-2}$$

where ε_x was either 10% or 20%. The average values of v_{xy} and v_{xz} are reported in Table 2.

Heating the compressed samples to temperatures near to the softening temperature of the foams (i.e. 220 °C)

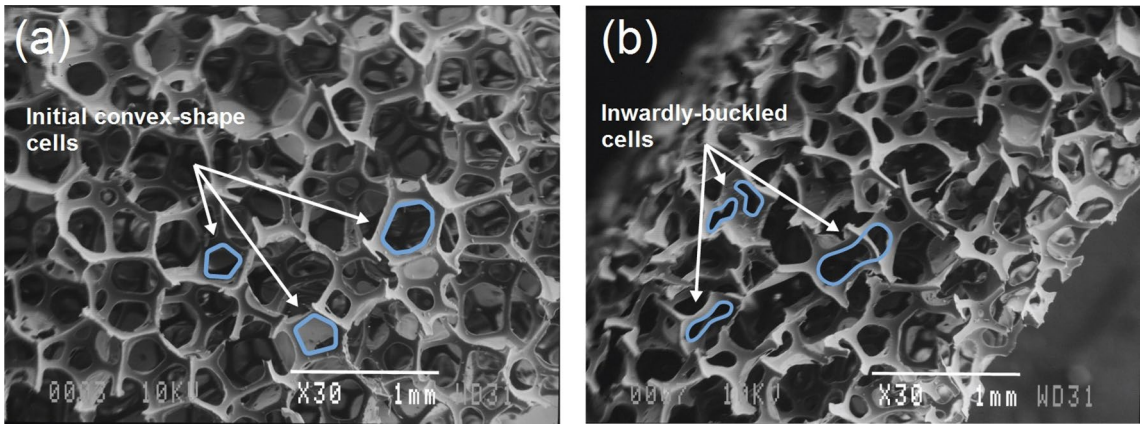

Fig. 4 SEM images of the **a** conventional and **b** auxetic foams in the *x–z* plane (i.e. within the thickness of the foam)

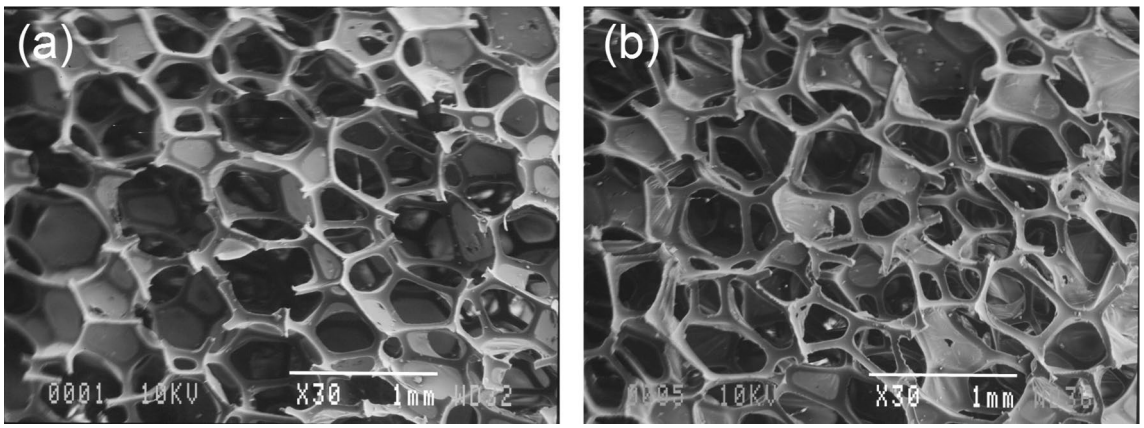

Fig. 5 SEM images of the **a** conventional and **b** auxetic foams in the *x–y* plane

Table 2 The *v* values of the processed samples (±95% Confidence Interval)

Test No	v_{xy} (ε_x = 10%)	v_{xy} (ε_x = 20%)	v_{xz} (ε_x = 10%)	v_{xz} (ε_x = 20%)
1	0.42 ± 0.10	0.46 ± 0.07	0.38 ± 0.13	0.48 ± 0.16
2	0.41 ± 0.08	0.56 ± 0.05	0.22 ± 0.09	0.51 ± 0.16
3	0.52 ± 0.11	0.64 ± 0.05	0.63 ± 0.04	0.76 ± 0.03
4	0.34 ± 0.08	0.40 ± 0.07	− 0.20 ± 0.02	− 0.10 ± 0.06
5	0.38 ± 0.07	0.52 ± 0.09	0.54 ± 0.03	0.71 ± 0.06
6	0.81 ± 0.04	0.96 ± 0.11	-0.35 ± 0.12	− 0.22 ± 0.01
7	0.52 ± 0.01	0.64 ± 0.02	0.56 ± 0.01	0.68 ± 0.09
8	0.52 ± 0.11	0.64 ± 0.07	0.76 ± 0.02	0.66 ± 0.16
9	0.60 ± 0.10	0.64 ± 0.01	0.87 ± 0.04	0.89 ± 0.04
10	0.48 ± 0.03	0.52 ± 0.04	0.58 ± 0.09	0.58 ± 0.07
11	0.78 ± 0.09	0.80 ± 0.11	0.82 ± 0.14	0.74 ± 0.01
12	0.66 ± 0.17	0.71 ± 0.04	0.68 ± 0.21	0.68 ± 0.13

reduced their thicknesses. The percentage of change in foam thickness (T_c) was defined using the following equation:

$$T_c = \frac{T_f - T_0}{T_0} \times 100 \quad (3)$$

where T_f is the final thickness of the foams. The T_c values are reported in Table 3. Also, changing the thickness of the samples changed their densities. The percentage of change in foam density (D_c) was defined using the following equations assuming that the variations in foam mass and surface area during the manufacturing process were negligible:

Table 3 The T_c, D_c and E value of processed samples (±95% Confidence Interval)

Test No	T_c (%)	D_c (%)	E (ε_x = 10%) (kPa)	E (ε_x = 20%) (kPa)
1	−13.0 ± 5.9	15.0 ± 7.4	94 ± 22	99 ± 28
2	−36.0 ± 3.9	56.5 ± 8.8	174 ± 4	201 ± 4
3	−8.5 ± 5.9	12.5 ± 10.8	165 ± 6	176 ± 21
4	−48.3 ± 1.9	93.5 ± 6.9	201 ± 4	187 ± 51
5	−5.2 ± 3.4	6.0 ± 3.9	135 ± 1	152 ± 3
6	−44.5 ± 8.5	81.0 ± 27.4	363 ± 100	443 ± 159
7	−8.0 ± 0.1	9.1 ± 0.1	128 ± 2	142 ± 2
8	−17.0 ± 9.8	21.0 ± 13.7	119 ± 55	135 ± 61
9	−3.5 ± 2.9	3.5 ± 2.9	207 ± 16	222 ± 8
10	−14.1 ± 0.1	16.1 ± 0.1	136 ± 30	137 ± 22
11	−12.3 ± 2.4	14.0 ± 3.9	224 ± 11	247 ± 24
12	−9.2 ± 3.4	10.0 ± 3.9	207 ± 34	226 ± 15

$$D_c = \frac{D_f - D_0}{D_0} * 100 \tag{4-1}$$

$$D_f = D_0 * {}^{T_0}/_{T_f} \tag{4-2}$$

where D_f is the final density of the foams. The D_c values are also reported in Table 3.

The load–displacement graphs of tensile tests were registered using a Zwick-Roell load-cell and a magnetic-based displacement sensor and are shown for one of the processed samples (i.e. sample number 9 with ε_x = 20%) in Fig. 6. The graphs were used to measure the amount of F to reach the deformation related to the desired ε_x. The next output of the study was E (i.e. Young's modulus of the foams). This property was calculated using the following equation [35]:

foams (i.e. the conventional foams before the thermo-mechanical procedure) with different D_0s and T_0s in ε_x of 10% and 20% and were reported in Table 4.

$$E = \frac{Tensile\ Stress}{\varepsilon_x} = \frac{F}{T_f * w * \varepsilon_x} \tag{5}$$

where w is the width of the sample (i.e. 60 mm). The E values for both ε_x values of 10% and 20% are reported in Table 3. Also, v_{xy}, v_{xz}, and E values were calculated for the conventional.

According to the results reported in Tables 2, 3, and 4, it is seen that two processed samples (i.e. samples 4 and 6) had a negative v_{xz} in both ε_x values of 10% and 20%. Also, all of the v_{xy} values remained positive. v_{xy} of 42% of processed samples reduced for both ε_x values. On the other hand, 42% of the processed samples at the ε_x of 10% and 58% of samples at the ε_x of 20% had fewer v_{xz} values than the related conventional ones. Also, the E value of 92% of processed samples increased in the tensile direction in both 10% and 20% ε_x values. The P value for the effect of each geometrical or processing

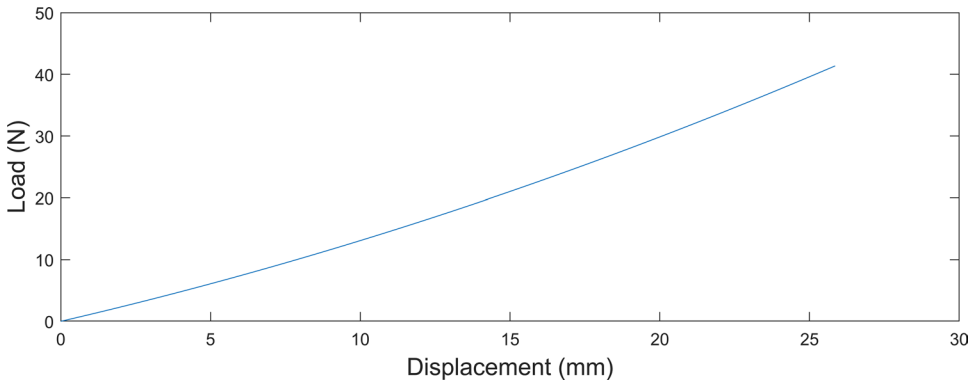

Fig. 6 The load–displacement graph of sample number 9

Table 4 The mechanical properties of conventional foams

D_0 (kg/m^3)	T_0 (mm)	Related Samples Numbers	v_{xy} (ε_x = 10%)	v_{xy} (ε_x = 20%)	v_{xz} (ε_x = 10%)	v_{xz} (ε_x = 20%)	E (ε_x = 10%) (kPa)	E (ε_x = 20%) (kPa)
20	5	6, 7, 8	0.56	0.66	0.52	0.53	100	111
20	20	2, 3, 5	0.36	0.48	0.43	0.51	128	137
40	5	1, 4, 10	0.43	0.48	0.39	0.63	100	113
40	20	9, 11, 12	0.62	0.69	0.73	0.77	205	218

Table 5 *P* values for the effect of each geometrical or processing parameter on the outputs

Output\Parameter	D_0	T_e	T_i	T_0	CR	RT
v_{xz} (ε_x = 10%)	0.688	0.000	0.006	0.010	0.011	0.419
v_{xz} (ε_x = 20%)	0.095	0.000	0.001	0.000	0.001	0.829
v_{xy} (ε_x = 10%)	0.120	0.695	0.111	0.032	0.042	0.001
v_{xy} (ε_x = 20%)	0.006	0.473	0.040	0.106	0.035	0.002
T_c	0.201	0.000	0.000	0.000	0.008	0.094
D_c	0.331	0.000	0.000	0.000	0.004	0.089
E (ε_x = 10%)	0.040	0.006	0.001	0.004	0.018	0.067
E (ε_x = 20%)	0.026	0.016	0.011	0.036	0.060	0.081

P values which are less than 0.05 (i.e. their effect is significant with 95% confidence) are underlined

Table 6 A summary of the influential parameters

	Outputs							
	v_{xz}		v_{xy}		T_c	D_c	E	
	ε_x = 10%	ε_x = 20%	ε_x = 10%	ε_x = 20%			ε_x = 10%	ε_x = 20%
Influential Parameters (*P* value < 0.05)	T_e	T_e	RT	RT	T_e	T_e	T_i	T_i
	T_i	T_0	T_0	D_0	T_i	T_i	T_0	T_e
	T_0	T_i	–	T_i	T_0	T_0	T_e	D_0
	CR	CR	–	–	CR	CR	CR	T_0
	–	–	–	–	–	–	D_0	–

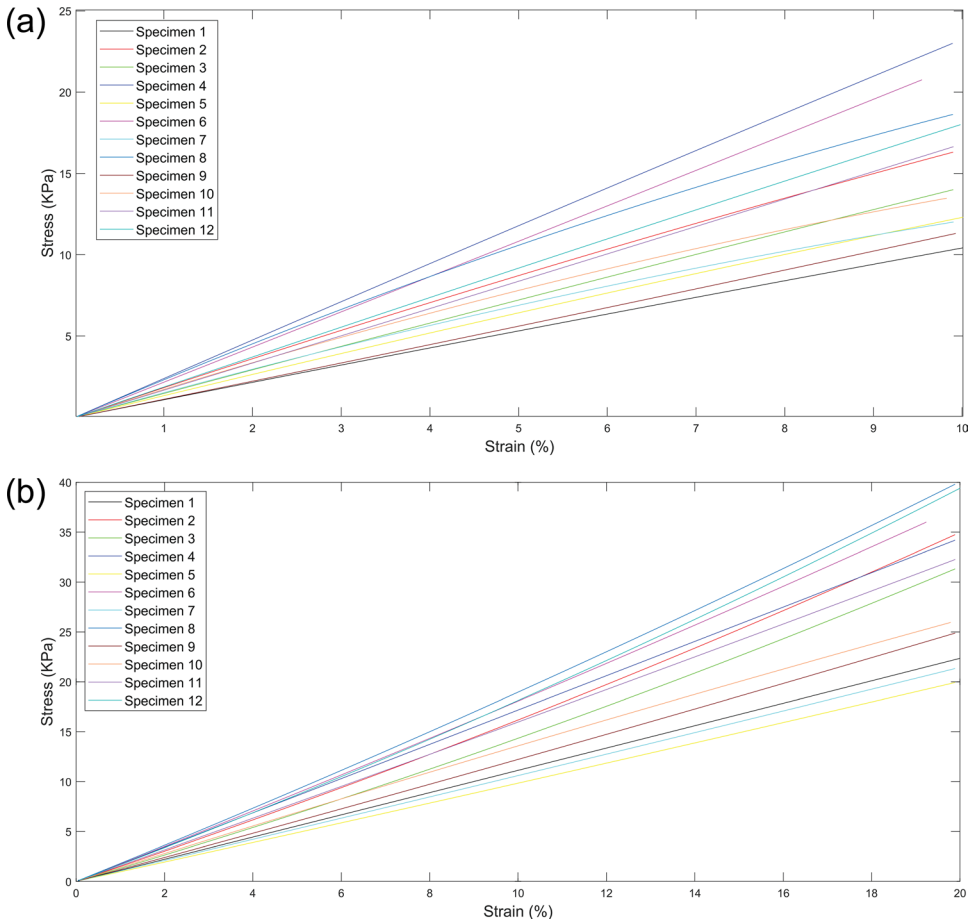

Fig. 7 stress–strain curve of foams in the tensile test at **a** 10% and **b** 20% strain

parameter was calculated using the ANOVA method and reported in Table 5. Table 6 summarizes the influential parameters on the properties of the foams that will be discussed in the following section.

3.3 Strain energy and v_{xz} calculation

As seen in Fig. 7, the slope of the stress–strain curves was linear and the foams were in the elastic region within the strain range of 20% consistent with the observations of ref. [21].

For 3D materials, the stress–strain equation is obtained from Hooke's law [36]:

$$\begin{bmatrix} \sigma_1 \\ \sigma_2 \\ \sigma_3 \end{bmatrix} = \begin{bmatrix} c_{11} & c_{12} & c_{13} \\ c_{12} & c_{22} & c_{23} \\ c_{13} c_{23} c_{33} \end{bmatrix} \begin{bmatrix} \varepsilon_1 \\ \varepsilon_2 \\ \varepsilon_3 \end{bmatrix} \tag{6}$$

Strain energy density is obtained from the following equation [36]:

$$u = \frac{1}{2} c_{ij} \varepsilon_i \varepsilon_j (i, j = 1, 2) \tag{7}$$

The strain energy can be also calculated from the area under the stress–strain curve. Since all the specimens were only compressed in the *z*-direction in the fabrication process, the mechanical properties of the other two directions of the samples were assumed to remain uniform in the energy calculations. By comparing the energies obtained from each sample in both ways (Fig. 8), it is seen that Eq. 7 was able to calculate the strain energy with high accuracy (i.e. within 7% of the measured values). Therefore, Eq. 7 could be used to calculate the strain energy density of auxetic foams in the elastic region.

The elastic stiffness constants of $c_{ij} (i, j = 1, 2, 3)$ can be obtained by applying small deformations and calculating the resultant stress vector or differentiating energy per unit volume, u, with respect to strain (see Eq. 7). Then, v_{xz} can be derived by the following expressions (the proof of this equation is given in "Appendix A"):

$$\nu_{xz} = \frac{c_{13}(c_{12} - c_{11})}{c_{13}^2 - c_{33} c_{11}} \tag{8}$$

After obtaining the elastic stiffness constants, the Poisson's ratio values of – 0.223 and – 0.326 for samples

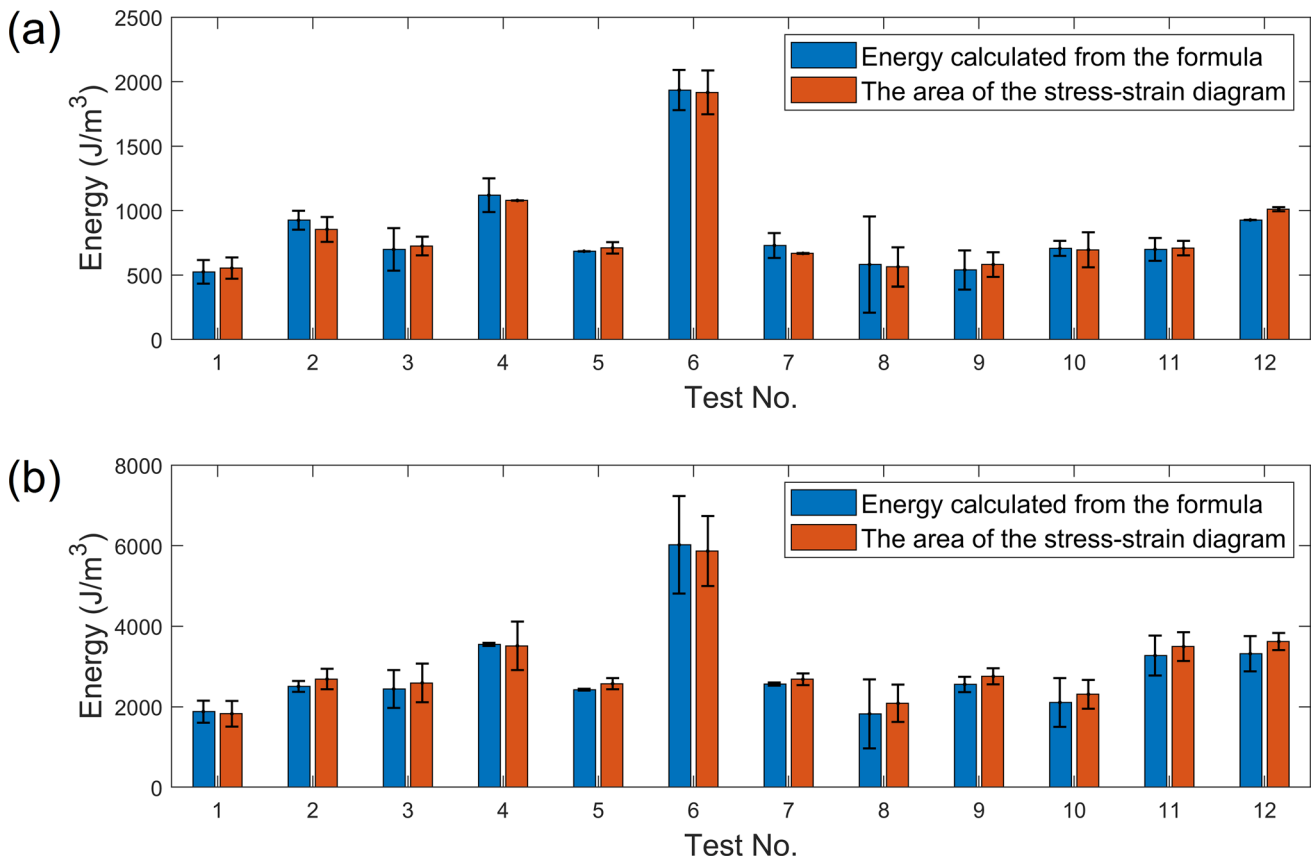

Fig. 8 Bar chart of the Strain energy density of the specimens obtained from Eq. 7 and the area under the stress–strain curve for strains of **a** 10% and **b** 20%

4 and 6 were obtained, respectively for the strain of 10%. These values are consistent with the ones that were experimentally measured (see Table 2).

4 Discussion

4.1 Effects of geometrical and processing parameters on v_{xz} changes

According to Table 5, the T_e, the T_0, the $T_{i,}$ and the *CR* applied to the foam had significant effects on the variations of v_{xz} for both ε_x values of 10% and 20%. It contradicts some previous observations that claimed only the *CR* value had a significant effect on *v*; i.e. no significant effect of the T_e level on *v* was observed [21, 31, 37, 38]. However, some investigations showed a substantial effect of T_e and T_i on this property [32, 33]. It is believed that these discrepancies in the observations of different studies are due to the interactional effects of some parameters on each other that were not incorporated in previous studies. The effects of D_0 and *RT* on v_{xz} were found insignificant.

The influence of each parameter on v_{xz} changes for different ε_x values is shown in Fig. 9. It can be seen that in both ε_x values, increasing the values of the T_e, T_i, and *CR* reduced the v_{xz}. It is believed that when these parameters increased, the foam formed to a permanent new re-entrant structure with a reduced *v* value. The effect of T_0 was the opposite so that when it increased, the amount of v_{xz} increased. It is believed that is because of the interactional effects of T_0 and processing parameters; as the T_0 increased, higher values of T_e, T_i, and *CR* should be applied to the samples to decrease their v_{xz} values. Also, it should be noted that the ε_x value did not influence the v_{xz} variations significantly and the results were almost the same for both ε_x values (*P* value = 0.847).

4.2 Effects of geometrical and processing parameters on v_{xy} changes

As reported in Table 5, the rest time, *RT*, between two heating stages had the most significant effect on the variations of v_{xy} for both values of ε_x. Also, T_0 and applied *CR* for ε_x of 10% and D_0, applied *CR*, and T_i for ε_x of 20% significantly affected the v_{xy} changes. Nevertheless, the T_e had no significant effect on v_{xy} variations in any of the ε_x values. Therefore, the effects of the varying parameters on v_{xy} changes were almost different from their effects on v_{xz} variations. It is believed that this difference was observed because the compression was only applied in *z* direction and the structure of the foam in the *y* direction did not significantly change during the thermo-mechanical procedure.

As seen in Fig. 10, T_i, T_0, and the applied *CR* had a direct relationship with the v_{xy} changes for both values of ε_x. But this correlation for the *RT* and foam D_0 was inverse. It could be noted that the changes that occurred in v_{xy} and v_{xz} could be somewhat independent of each other by changing the initial and processing parameters. As reported in Table. 5 and Fig. 10, the most effective parameters on v_{xy} variations were the *RT* and D_0 that did not affect v_{xz}. Also, the most influential factors on v_{xz} changes had less effects on v_{xy} variations. It can be seen in Fig. 10 that the effect of the other parameters was almost independent of the ε_x value (*P* value = 0.747).

4.3 Effects of geometrical and processing parameters on T_c and D_c

According to Table 5, the influential parameters on the T_c and D_c of the samples were similar to those that affected the value of v_{xz}. T_e, T_i, T_0, and applied *CR* had the most significant effects on both T_c and D_c. As it is shown in Fig. 11, increasing T_e, $T_{i,}$ and also the applied *CR* caused T_c to become more negative and, therefore, T_f value

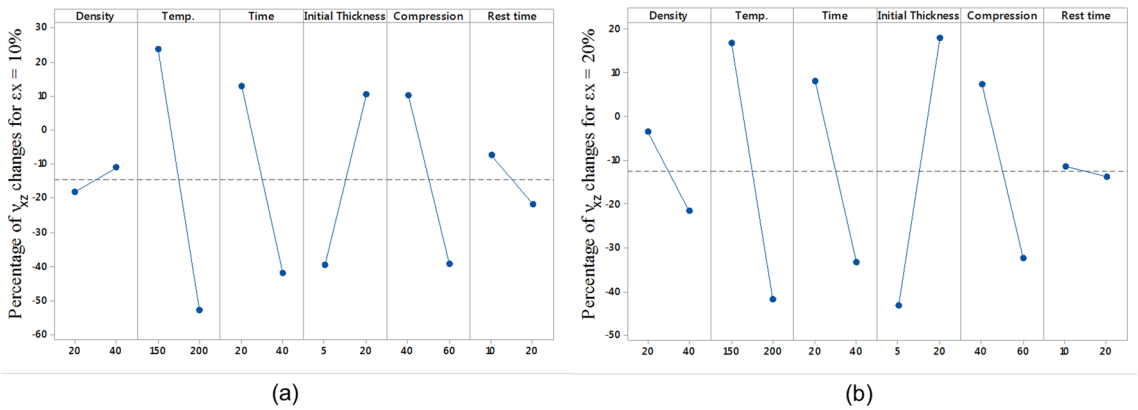

Fig. 9 Effect of different parameters on the v_{xz} changes for ε_x of **a** 10% and **b** 20%

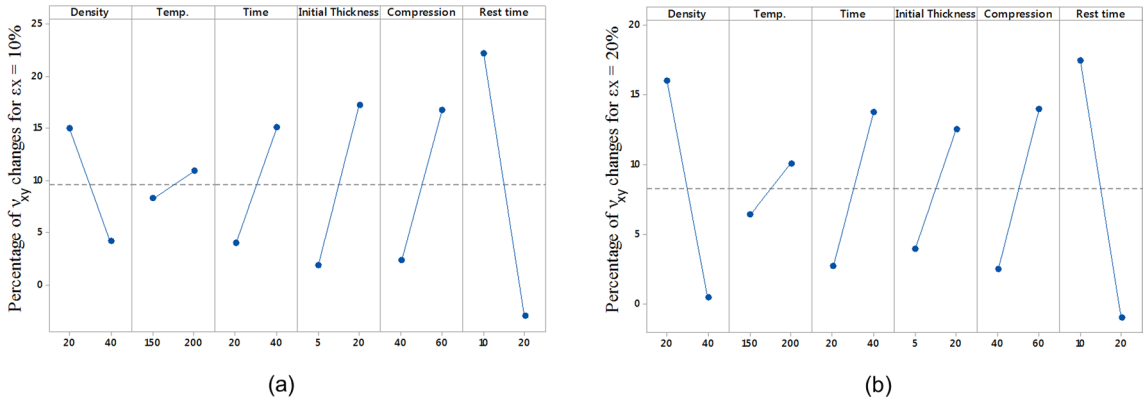

Fig. 10 Effect of different parameters on the v_{xy} changes in the ε_x of **a** 10% and **b** 20%

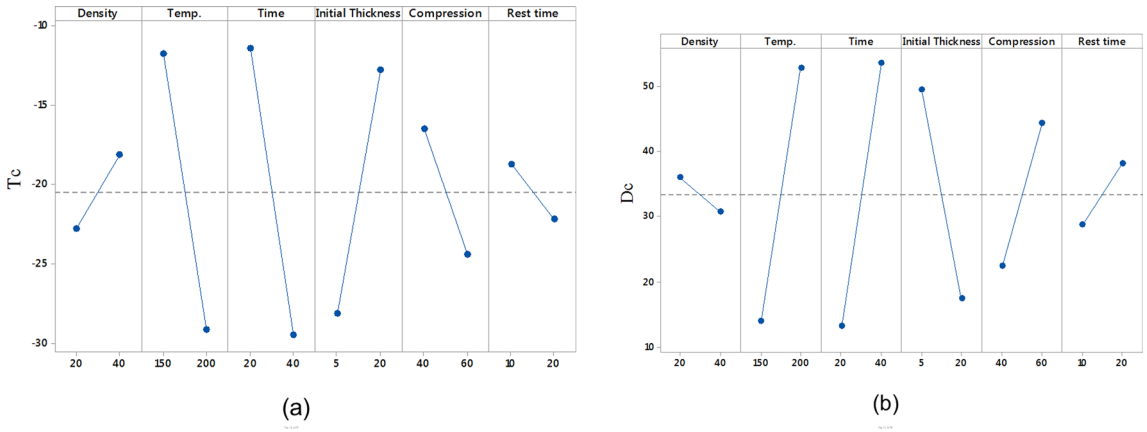

Fig. 11 Effect of different parameters on **a** T_c and **b** D_c

decreased. It is believed that applying compression in temperature near the softening point of the foams (i.e. 220 °C) would cause plastic deformation in them. So when the T_e increased to a temperature near the softening temperature (i.e. 200 °C or 150 °C) and also *CR* and T_i increased, the T_c value (i.e. the plastic deformation of foams) would grow too. But the effect of T_0 on T_c was the opposite; when T_0 increased, the T_c value became closer to zero and the permanent deformation ratio in the thickness of the foam decreased. It is hypothesized that this is due to the interactional effects of T_0 and other effective parameters that should be investigated in the future.

Also, it is shown in Fig. 11 that the effects of T_e, T_i, T_0, and applied *CR* on D_c opposed their effects on T_c. This was predictable due to Eqs. 4-1 and 4-2 where it was shown that with a decline in the amount of T_f (i.e. T_c being more negative), the D_f and D_c would increase. It could be also observed that when the T_e and T_i were elevated or the T_0 value declined, the D_c value of the samples increased. Also, consistent with the observations of ref. [31], D_c and D_f values became larger when the applied *CR* increased. It should be noted that no significant effect of D_0 on the D_c value was observed.

4.4 Effects of geometrical and processing parameters on *E* changes

The statistical analysis reported in Table 5 showed that for both ε_x values of 10% and 20%, the most influential parameters on the variations of *E* value were T_e, T_i, T_0, and D_0 of the foams. Also, the applied *CR* in the ε_x value of 10% affected the changes in the *E* value in the thermo-mechanical procedure significantly. But the *RT* did not affect *E* variations significantly in any strain value. Figure 12 shows that the changes in the *E* value of the samples are directly related to T_e and T_i and also the applied *CR* on the foam. This is consistent with the findings of Refs. [31, 33, 37] where an increase in *CR* was shown to increase the *E* value. It is hypothesized that with the growth of these parameters (i.e. reduction of T_f), the processed foam would

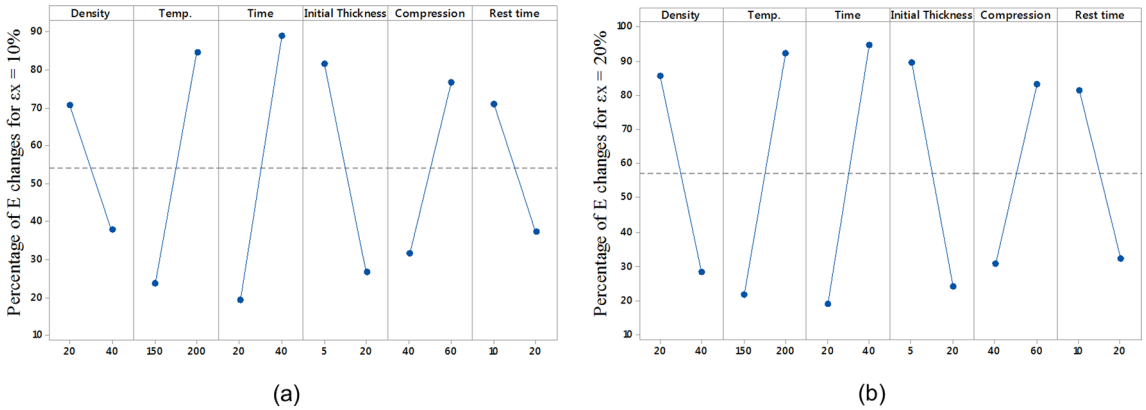

Fig. 12 Effect of different parameters on the E changes in the ε_x of **a** 10% and **b** 20%

have a more compact and denser structure (see Sect. 4.3) and the amount of porosity in the structure would reduce, rendering an increase in the E variations and so the E value.

Figure 12 shows a direct relationship between T_e and changes of E. But previous investigations have reported different conclusions on this correlation [31, 32]. It is believed that if the T_e increases to a value more than the softening temperature, the foam will enter the flow temperature region and will have plastic behavior and its E value will reduce [27]. On the other hand, the E variations were found to be inversely related to the T_0 and the D_0 of samples. It is believed that with increasing the D_0 of samples and reduction of their porosity, their behavior would become closer to elastic conditions and, hence, the changes in their E value would decrease.

Finally, it is seen in Fig. 12 that the ε_x value did not significantly change the effect of the parameters on E (P value = 0.839). It is believed that this is due to the elastic behavior of conventional and processed PU foams in ε_x values of lower than 20% [39]. This behavior of the foam material is also illustrated in Fig. 6 that shows an almost linear relationship between the applied load and the displacement of the foam. According to Tables 5 and 6, it could be observed that the parameters that affect the E and v_{xz} variations are the same. This implies these two properties could be dependent on each other. Also, Figs. 9 and 12 show that the effect of parameters on the E was the opposite of their effect on the v_{xz}.

4.5 Comparison of strain energies and Poisson's ratios in theoretical and experimental calculations

It was observed that the strain energy value in foams with a negative Poisson's ratio (i.e. samples No. 4 and 6) was higher than that for the other specimens. However, the foams with a reduced Poisson's ratio showed increased strain energy compared to the conventional specimens. The difference of the calculated Poisson's ratio with the measured value was approximately 8% for samples No. 4 and 6. It shows that Poisson's ratio of auxetic foams can be obtained using a stress–strain curve of the tensile test.

4.6 Limitations of the study and future studies

This investigation aimed to observe the effects of six different factors on several output properties such as v in two directions and the E value of the products. A large number of experiments were performed and each sample required a long time for the thermo-mechanical procedure. Also, performing the tensile test on each sample in two ε_x values and data acquisition with the DIC method in two directions increased the required time to perform each test. Therefore, this study used a Plackett–Burman design of experiments method to reduce the number of the required tests that were suitable to detect the most effective parameters on the results. Also, this study identified the factors that had almost insignificant effects on the desired properties to eliminate them from future studies. Another experiment design would be needed to investigate the exact effect and interactions of the identified significant parameters to optimize the properties.

5 Conclusions

The main goal of this study was to detect influential parameters and compare their effects on different mechanical properties of PU foams after the thermo-mechanical process of manufacturing auxetic materials. The tensile test and DIC of the samples were used to obtain stress–strain curve, v and E values for all specimens. It was concluded that T_0, T_e, T_i, and applied CR had the most significant effects on v_{xz}, E, and D_c. But the effect of these parameters

on E was the opposite of their effect on v_{xz} and D_c. On the other hand, RT, T_0, and CR had the most significant effects on v_{xy}. Generally, the most effective parameters on almost all of these outputs (i.e. v_{xz}, v_{xy}, E, T_c, and D_c) were T_e, T_i, T_0, and applied CR on them during the heating procedure. Strain energy values were calculated in both experimental measurements and theoretical relationships, and the two auxetic specimens showed a remarkably higher stored energy compared to the non-auxetic ones. These investigations on the effective parameters would help to optimize the final mechanical properties (i.e. cost function) of the PU foams such as v_{xz}, E, or energy dissipation depending on the desired applications.

Authors contributions NHZA: Methodology, Software, Writing original draft, Data curation, Investigation. AN: Project administration, Supervision, review & editing, Conceptualization. MM: Conceptualization, Data curation, Formal analysis, Methodology, Writing original draft, Software. NH: Formal analysis, Investigation, Methodology, Software, Writing original draft. SN: Writing original draft, Investigation, Methodology. PRB: Formal analysis, Methodology.

Funding This research did not receive any specific grant from funding agencies in the public, commercial, or not-for-profit sectors.

Availability of data and material All authors make sure that all data and materials as well as software application or custom code support their published claims and comply with field standards.

Data availability The datasets generated during and/or analysed during the current study are not publicly available due to the large amount of data but are available from the corresponding author on reasonable request.

Code availability Not applicable.

Declarations

Conflicts of interest Each author certifies that he or she has no commercial associations (e.g., consultancies, stock ownership, equity interest, patent/licensing arrangements, etc.) that might pose a conflict of interest in connection with the submitted article.

Ethics approval Not applicable.

Consent to participate Not applicable.

Consent for publication Not applicable.

Appendix A

By convention, the 9 elastic constants in orthotropic constitutive equations are comprised of 3 Young's moduli, E_x, E_y, E_z, 3 Poisson's ratios, v_{yz}, v_{zx}, v_{xy}, and 3 shear moduli, G_{yz}, G_{zx}, G_{xy} that are assumed to be zero. Therefore, the stiffness matrix takes the form:

$$\begin{bmatrix}\sigma_{xx}\\ \sigma_{yy}\\ \sigma_{zz}\end{bmatrix}=\begin{bmatrix}\frac{1-v_{yz}v_{zy}}{E_yE_z\Delta} & \frac{v_{yx}+v_{zx}v_{yz}}{E_yE_z\Delta} & \frac{v_{zx}+v_{yx}v_{zy}}{E_yE_z\Delta}\\ \frac{v_{xy}+v_{xy}v_{zy}}{E_zE_x\Delta} & \frac{1-v_{zx}v_{xz}}{E_zE_x\Delta} & \frac{v_{zy}+v_{zx}v_{xy}}{E_zE_x\Delta}\\ \frac{v_{xz}+v_{xy}v_{yz}}{E_xE_y\Delta} & \frac{v_{yz}+v_{xz}v_{yx}}{E_xE_y\Delta} & \frac{1-v_{xy}v_{yx}}{E_xE_y\Delta}\end{bmatrix}\begin{bmatrix}\varepsilon_{xx}\\ \varepsilon_{yy}\\ \varepsilon_{zz}\end{bmatrix} \tag{A1}$$

where:

$$\Delta=\frac{1-v_{xy}v_{yx}-v_{yz}v_{zy}-v_{zx}v_{xz}-2v_{xz}v_{yz}v_{zx}}{E_xE_yE_z} \tag{A2}$$

The mechanical properties (Young's modulus and Poisson's ratios) are the same in both the x and y directions.

$$v_{xy}=v_{yx}, v_{zx}=v_{zy}, v_{xz}=v_{yz}, E_x=E_y \tag{A3}$$

Therefore, Hoke's low becomes:

$$\begin{bmatrix}\sigma_{xx}\\ \sigma_{yy}\\ \sigma_{zz}\end{bmatrix}=\begin{bmatrix}\frac{1-v_{xz}v_{zx}}{E_xE_z\Delta} & \frac{v_{yx}+v_{zx}v_{xz}}{E_xE_z\Delta} & \frac{v_{zx}+v_{yx}v_{zx}}{E_xE_z\Delta}\\ \frac{v_{xy}+v_{xy}v_{zx}}{E_zE_x\Delta} & \frac{1-v_{zx}v_{xz}}{E_zE_x\Delta} & \frac{v_{zx}+v_{zx}v_{xy}}{E_zE_x\Delta}\\ \frac{v_{xz}+v_{xy}v_{xz}}{E_xE_x\Delta} & \frac{v_{yz}+v_{xz}v_{yx}}{E_xE_x\Delta} & \frac{1-v_{xy}v_{yx}}{E_xE_x\Delta}\end{bmatrix}\begin{bmatrix}\varepsilon_{xx}\\ \varepsilon_{yy}\\ \varepsilon_{zz}\end{bmatrix} \tag{A4}$$

where:

$$\frac{v_{yz}}{E_y}=\frac{v_{zy}}{E_z}, \frac{v_{zx}}{E_z}=\frac{v_{xz}}{E_x}, \frac{v_{xy}}{Ex}=\frac{v_{yx}}{E_y} \tag{A5}$$

Then:

$$\begin{bmatrix}\sigma_{xx}\\ \sigma_{yy}\\ \sigma_{zz}\end{bmatrix}=\begin{bmatrix}\frac{1}{E_xE_z\Delta}-\frac{v_{xz}^2}{E_x^2\Delta} & \frac{v_{yx}}{E_xE_z\Delta}+\frac{v_{xz}^2}{E_x^2\Delta} & \frac{v_{xz}(1+v_{yx})}{E_x^2\Delta}\\ \frac{v_{yx}}{E_zE_x\Delta}+\frac{v_{xy}^2}{E_z^2\Delta} & \frac{1-v_{zx}v_{xz}}{E_zE_x\Delta} & \frac{v_{zx}+v_{zx}v_{xy}}{E_zE_x\Delta}\\ \frac{v_{xz}(1+v_{yx})}{E_x^2\Delta} & \frac{v_{xz}(1+v_{yx})}{E_x^2\Delta} & \frac{1-v_{yx}^2}{E_x^2\Delta}\end{bmatrix}\begin{bmatrix}\varepsilon_{xx}\\ \varepsilon_{yy}\\ \varepsilon_{zz}\end{bmatrix} \tag{A6}$$

Also, the stiffness matrix is symmetric as follows:

$$\begin{bmatrix}\sigma_1\\ \sigma_2\\ \sigma_3\end{bmatrix}=\begin{bmatrix}c_{11} & c_{12} & c_{13}\\ c_{12} & c_{11} & c_{13}\\ c_{13} & c_{13} & c_{33}\end{bmatrix}\begin{bmatrix}\varepsilon_1\\ \varepsilon_2\\ \varepsilon_3\end{bmatrix} \tag{A7}$$

Therefore:

$$c_{11}=c_{22} \tag{A8}$$

$$c_{12}=c_{21} \tag{A9}$$

$$c_{13}=c_{23}=c_{31}=c_{32} \tag{A10}$$

Thus, Eq. 8 is obtained:

$$\nu_{xz} = \frac{c_{13}(c_{12} - c_{11})}{c_{13}^2 - c_{33}c_{11}} \quad (8)$$

References

1. Moroney C, Alderson A, Allen T, Sanami M, Venkatraman P (2018) The application of auxetic material for protective sports apparel. Proceedings 2(6):251. https://doi.org/10.3390/proceedings2060251
2. Majewski A, Smardzewski J (2015) Models for elastic deformation of auxetic honeycomb with triangular cells. In: XXVIIth International Conference Research for Furniture Industry
3. Donoghue JP, Alderson KL, Evans KE (2009) The fracture toughness of composite laminates with a negative Poisson's ratio. Phys Status Solidi Basic Res 246:2011–2017. https://doi.org/10.1002/pssb.200982031
4. Saxena KK, Das R, Calius EP (2016) Three decades of auxetics research—materials with negative Poisson's ratio: a review. Adv Eng Mater 18:1847–1870. https://doi.org/10.1002/adem.201600053
5. Strek T, Jopek H, Nienartowicz M (2015) Dynamic response of sandwich panels with auxetic cores. Phys Status Solidi 252:1540–1550. https://doi.org/10.1002/pssb.201552024
6. Imbalzano G, Linforth S, Ngo TD, Lee PVS, Tran P (2018) Blast resistance of auxetic and honeycomb sandwich panels: Comparisons and parametric designs. Compos Struct 183:242–261. https://doi.org/10.1016/j.compstruct.2017.03.018
7. Lakes RS (1987) Polyhedron cell structure and method of making same, Int. Patent, Publ. No. WO88/00523
8. Love A (1944) A treatise on the mathematical theory of elasticity. Dover Publications, New York
9. Alderson KL, Evans KE (1992) The fabrication of microporous polyethylene having a negative Poisson's ratio. Polymer (Guildf) 33:4435–4438. https://doi.org/10.1016/0032-3861(92)90294-7
10. Gunton DJ, Saunders GA (1972) The Young's modulus and Poisson's ratio of arsenic, antimony and bismuth. J Mater Sci 7:1061–1068. https://doi.org/10.1007/BF00550070
11. Li Y (1976) The anisotropic behavior of Poisson's ratio, Young's modulus, and shear modulus in hexagonal materials. Phys Status Solidi 38:171–175. https://doi.org/10.1002/pssa.2210380119
12. Krasavin VV, Krasavin AV (2014) Auxetic properties of cubic metal single crystals. Phys Status Solidi Basic Res 251:2314–2320. https://doi.org/10.1002/pssb.201451129
13. Yeganeh-Haeri A, Weidner DJ, Parise JB (1992) Elasticity of α-cristobalite: a silicon dioxide with a negative Poisson's ratio. Science (80-) 257:650–652. https://doi.org/10.1126/science.257.5070.650
14. Williams JL, Lewis JL (1982) Properties and an anisotropic model of cancellous bone from the proximal tibial epiphysis. J Biomech Eng 104:50–56. https://doi.org/10.1115/1.3138303
15. Evans KE, Alderson A (2000) Auxetic materials: functional materials and structures from lateral thinking! Adv Mater 12:617–628. https://doi.org/10.1002/(SICI)1521-4095(200005)12:9%3c617::AID-ADMA617%3e3.0.CO;2-3
16. Grima JN, Evans KE (2000) Auxetic behavior from rotating squares. J Mater Sci Lett 19:1563–1565. https://doi.org/10.1023/A:1006781224002
17. Grima JN, Alderson A, Evans KE (2004) Negative Poisson'S ratios from rotating rectangles. Comput Methods Sci Technol 10:137–145. https://doi.org/10.12921/cmst.2004.10.02.137-145
18. Grima JN, Gatt R, Farrugia PS (2008) On the properties of auxetic meta-tetrachiral structures. Phys Status Solidi Basic Res 245:511–520. https://doi.org/10.1002/pssb.200777704
19. Lim T-C (2019) Metamaterials with Poisson's ratio sign toggling by means of microstructural duality. SN Appl Sci 1:176. https://doi.org/10.1007/s42452-019-0185-1
20. Lakes R (1987) Foam structures with a negative Poisson's ratio. Science (80-) 235:1038–1040. https://doi.org/10.1126/science.235.4792.1038
21. Bianchi M, Scarpa FL, Smith CW (2008) Stiffness and energy dissipation in polyurethane auxetic foams. J Mater Sci 43:5851–5860. https://doi.org/10.1007/s10853-008-2841-5
22. Li Y, Zeng C (2016) Room-temperature, near-instantaneous fabrication of auxetic materials with constant Poisson's ratio over large deformation. Adv Mater 28:2822–2826. https://doi.org/10.1002/adma.201505650
23. Constantinescu DM, Apostol DA (2020) Performance and efficiency of polyurethane foams under the influence of temperature and strain rate variation. J Mater Eng Perform 29:3016–3029. https://doi.org/10.1007/s11665-020-04860-4
24. Deschanel S, Vanel L, Vigier G, Godin N, Ciliberto S (2006) Statistical properties of microcracking in polyurethane foams under tensile test, influence of temperature and density. Int J Fract 140:87–98. https://doi.org/10.1007/s10704-006-0051-1
25. Linul E, Şerban DA, Marsavina L, Sadowski T (2017) Assessment of collapse diagrams of rigid polyurethane foams under dynamic loading conditions. Arch Civ Mech Eng 17:457–466. https://doi.org/10.1016/j.acme.2016.12.009
26. Alderson K, Alderson A, Ravirala N, Simkins V, Davies P (2012) Manufacture and characterisation of thin flat and curved auxetic foam sheets. Phys Status Solidi Basic Res 249:1315–1321. https://doi.org/10.1002/pssb.201084215
27. Lisiecki J (2017) Auxetic polyurethane foams—method for determining a softening point. Aviat Adv Maint 40:5–38. https://doi.org/10.1515/afit-2017-0007
28. Duncan O, Allen T, Foster L, Senior T, Alderson A (2017) Fabrication, characterisation and modelling of uniform and gradient auxetic foam sheets. Acta Mater 126:426–437. https://doi.org/10.1016/j.actamat.2017.01.004
29. Grima JN, Alderson A, Evans KE (2005) An alternative explanation for the negative Poisson's ratios in auxetic foams. J Phys Soc Japan 74:1341–1342. https://doi.org/10.1143/JPSJ.74.1341
30. Sanami M, Alderson A, Alderson KL, McDonald SA, Mottershead B, Withers PJ (2014) The production and characterization of topologically and mechanically gradient open-cell thermoplastic

foams. Smart Mater Struct 23:055016. https://doi.org/10.1088/0964-1726/23/5/055016
31. Bianchi M, Frontoni S, Scarpa F, Smith CW (2011) Density change during the manufacturing process of PU-PE open cell auxetic foams. Phys Status solidi 248:30–38. https://doi.org/10.1002/pssb.201083966
32. Duncan O, Clegg F, Essa A, Bell A, Foster L, Allen T, Alderson A (2018) Effects of heat exposure and volumetric compression on Poisson's ratios, young's moduli, and polymeric composition during thermo-mechanical conversion of auxetic open cell polyurethane foam. Phys status solidi. https://doi.org/10.1002/pssb.201800393
33. Najarian F, Alipour R, Nejad AF, Razavykia A (2018) Multi-objective optimization of converting process of auxetic foam using three different statistical methods. Measurement 119:108–116. https://doi.org/10.1016/j.measurement.2018.01.064
34. Novak N, DobnikDubrovski P, Borovinšek M, Vesenjak M, Ren Z (2020) Deformation behaviour of advanced textile composites with auxetic structure. Compos Struct 252:112761. https://doi.org/10.1016/j.compstruct.2020.112761
35. Beer FP, Johnston ER, DeWolf JT, Mazurek DF (1992) Mechanics of materials, 7th edn. McGraw-Hill's, New York
36. Lai WM, Rubin DH, Rubin D, Krempl E (2009) Introduction to continuum mechanics. Butterworth-Heinemann
37. Lisiecki J, Kłysz S, TB, Nowakowski D, Reymer P (2014) Auxetic polyurethane foams-manufacturing and testing. pp 217–220
38. Alderson A, Davies PJ, Alderson KIML, Smart GM (2005) The effects of processing on the topology and mechanical properties of negative poisson's ratio foams. In: ASME International Mechanical Engineering Congress and Exposition. pp 1–8
39. Scarpa F, Ciffo LG, Yates JR (2003) Dynamic properties of high structural integrity auxetic open cell foam. Smart Mater Struct 13:49